Lawrence Berkeley National Laboratory
Recent Work

Title
SURVEY OF THE (a,2He) REACTION ON lp- AND 2sld-SHELL NUCLEI

Permalink
https://escholarship.org/uc/item/14b3k2h1

Author
Jahn, R.

Publication Date
1978-03-01

SURVEY OF THE $(\alpha, {}^2\text{He})$ REACTION ON 1p- AND
2s1d-SHELL NUCLEI

R. Jahn, D. P. Stahel, G. J. Wozniak,
R. J. de Meijer, and Joseph Cerny

March 1978

DISCLAIMER

SURVEY OF THE (α,^{2}He) REACTION ON 1p- AND 2s1d-SHELL NUCLEI

R. Jahn[+], D. P. Stahel, G. J. Wozniak, R. J. de Meijer[++]

and Joseph Cerny

Department of Chemistry and
Lawrence Berkeley Laboratory,
University of California,
Berkeley, California 94720

March 1978

ABSTRACT

A ^{2}He detection system has been developed and used to investigate the (α,^{2}He) reaction at bombarding energies of 55 and 65 MeV on targets of ^{12}C, ^{13}C, ^{14}N, ^{15}N, ^{16}O, ^{18}O, ^{20}Ne, ^{22}Ne, ^{24}Mg, ^{26}Mg, ^{28}Si, ^{29}Si, ^{32}S, ^{36}Ar, ^{38}Ar, and ^{40}Ca. Preferential population of two-neutron states with dominant $(d_{5/2})^2_4$, $(d_{3/2}f_{7/2})_5$ and $(f_{7/2})^2_6$ character was observed. A linear A-dependence of the binding energies of the $J^\pi = 5^-$ and 6^+ states was obtained. This systematic behavior is well described by the Bansal-French model, using the parameters a = - 0.30 MeV and b = 2.6 MeV. Simple shell-model calculations for the 2n configurations are in good agreement with the experimental data.

$$\begin{array}{|l|}
\hline
\text{NUCLEAR REACTIONS } {}^{12}\text{C, } {}^{13}\text{C, } {}^{14}\text{N, } {}^{15}\text{N, } {}^{16}\text{O, } {}^{18}\text{O, } {}^{20}\text{Ne,} \\
{}^{22}\text{Ne, } {}^{26}\text{Mg, } {}^{28}\text{Si, } {}^{29}\text{Si, } {}^{32}\text{S, } {}^{36}\text{Ar, } {}^{38}\text{Ar, } (\alpha,{}^2\text{He}), \\
\text{E = 65 MeV and } {}^{24}\text{Mg, } {}^{40}\text{Ca, } (\alpha,{}^2\text{He}), \text{ E = 55 MeV.} \\
\text{Measured } \sigma(E_f,\theta), \text{ deduced } E_x \text{ and } J^\pi \text{ systematics.} \\
\hline
\end{array}$$

I. INTRODUCTION

A recent study of the $(\alpha, {}^2\text{He})$ reaction on lp-shell targets[1] has demonstrated that this reaction selectively populates two-neutron states of high spin in the final nuclei. Results from this reaction can be compared with those from the (α, d) reaction on light nuclei.[2-5] The selectivity of the (α, d) reaction at E_α of about 50 MeV for $(1d_{5/2})^2_5$ and $(1f_{7/2})^2_7$ transfers is due to its large negative Q-values which kinematically favor transitions to high-spin states, a good overlap of the relative s motion of the neutron-proton pair with the relative s motion in the projectile and the large spectroscopic factors involved in the transitions. Since the $(\alpha, {}^2\text{He})$ reaction at comparable bombarding energies has similar properties, one expects to observe strong population of states in which two neutrons are coupled to maximum allowed spin, i.e. $(1d_{5/2})^2_4$ and $(1f_{7/2})^2_6$. Because the analogous (t,p) reaction has not been investigated under similar kinematic conditions due to the lack of high energy triton beams and because only a few heavy-ion 2n transfer reactions have been reported[6,7], only a small number of these 2n high-spin states are known in light nuclei.

In the present study the $(\alpha, {}^2\text{He})$ reaction has been observed over a wide range of lp- and 2sld-shell target nuclei, thus permitting a broad search for 2n states of high spin. Our intention has been to provide an initial survey and not, in general, to obtain detailed angular distributions. Targets of ${}^{12}\text{C}$, ${}^{13}\text{C}$, ${}^{14}\text{N}$, ${}^{15}\text{N}$, ${}^{16}\text{O}$, ${}^{18}\text{O}$, ${}^{20}\text{Ne}$, ${}^{22}\text{Ne}$, ${}^{24}\text{Mg}$, ${}^{26}\text{Mg}$, ${}^{28}\text{Si}$, ${}^{29}\text{Si}$, ${}^{32}\text{S}$, ${}^{36}\text{Ar}$, ${}^{38}\text{Ar}$ and ${}^{40}\text{Ca}$ have been bombarded with 55 and 65 MeV α-particles. The ${}^2\text{He}$ spectra which have been obtained establish the selectivity of the $(\alpha, {}^2\text{He})$ reaction and its usefulness as an important spectroscopic tool for locating 2n states of high spin.

In Sections II and III the ^{2}He detection system and the experimental procedure are discussed. Energy spectra for each target are presented in Sec. IV which is divided into two parts describing separately the results on 1p-shell and 2s1d-shell targets. In Sec. V the data are compared with simple shell-model calculations. Finally, a summary is presented in Sec. VI.

II. THE ^{2}He DETECTION SYSTEM

The unbound reaction product ^{2}He can be identified by measuring its

two breakup protons in coincidence. Although this detection procedure is

similar to the one used in characterizing the unbound ^{8}Be nuclide via its

two decay α-particles,[8] the breakup energy of ^{2}He does not originate from

the decay of a narrow state, as in the case of ^{8}Be, but rather from a final

state interaction (FSI) distribution as has been observed in reactions such

as ^{2}H(^{3}He,t)2p (Ref. 9). The distribution of the relative energy ε of the

two protons in their c.m. system is usually described by the Watson-Migdal

formalism.[10,11] It peaks at $\varepsilon \approx$ 400 keV and falls off for higher values

with a slope of approximately $1/\varepsilon$. The detection geometry was therefore

arranged to yield the optimal efficiency for events having breakup energies

near this peak value.

The detection of ^{2}He via its breakup protons with reasonable

efficiency is facilitated by the fact that the transformation of the

isotropic breakup of ^{2}He in its c.m. to the laboratory system results in

a focussing of the breakup protons into a cone. The maximum opening angle

of this cone, β_{max}, is defined by ε and the ^{2}He laboratory energy E and

is given by $\beta_{max} = 2 \arctan (\varepsilon/E)^{1/2}$. This transformation also leads to

a concentration of breakup protons near the edge of the cone. Therefore,

in order to get optimum detection efficiency, it is important that the two-

proton acceptance angle of the detector be at least as large as the maximum

^{2}He breakup angle, which, for example, is 11.4° for E = 40 MeV and

ε = 400 keV. On the other hand, energy resolution considerations require

a small horizontal ^{2}He acceptance angle, in order to minimize kinematic

broadening. A good compromise between efficiency and energy resolution
was obtained by detecting the protons in a pair of vertically arranged
detector telescopes, each with a solid angle of about 6 msr. With this
configuration, a reasonable efficiency ($\sim$ 1%) was achieved as a result of
the large vertical acceptance angle and adequate energy resolution
(300-600 keV FWHM) was obtained by limiting the horizontal acceptance
angle.

Figure 1(a) shows a schematic diagram of the detection system which
consisted of two large solid-angle counter telescopes collimated by 8 mm
wide and 10 mm high slits which were separated by a 10 mm high central
post. At 11 cm from the target, this system subtended a 15° vertical and
a 4° horizontal acceptance angle. For the gas target measurements, a 3 mm
wide vertical slit (front gas collimator) was located at a distance of
4 cm from the center of the gas cell. Each telescope consisted of a 380 μm
phosphorus diffused silicon ΔE counter, a 5 mm Si(Li) E counter and a 5 mm
Si(Li) veto counter, the last being employed to reject events that traversed
the ΔE-E system.

Identification of protons in each ΔE telescope using standard
analog circuitry, coupled with a fast coincidence requirement between
events occuring in the two ΔE counters, was required to characterize
the ^{2}He events. In order to minimize the charge collection time in the
ΔE counters, a high bias voltage (2V/μm) was maintained. By using low
capacity cables and fast/slow preamplifiers an electronic time resolution
of $\sim$ 200 ps was achieved. Figure 1(b) shows the time-of-flight difference
(ΔTOF) distributions of observed proton coincidences from the reaction
^{13}C(α,^{2}He)^{15}C at Θ_{lab} = 13°. The observed full width at half maximum is

about 1.1 ns, which is in good agreement with calculations based on the

assumption of ^{2}He breakup. Since the width of a single beam burst was

10 ns, random coincidences were substantially reduced by setting a 3 ns

wide window around the ^{2}He peak in the 20 ns wide ΔTOF spectrum. Fast pileup

rejection permitted a high count rate (32,000 s^{-1}) in each ΔE counter,

with an associated overall system dead time of about 20%.

The ^{2}He detection efficiency is a function of the detector geometry,

the relative two-proton energy ε and the ^{2}He energy E. It was calculated

with the program EFFCR,[12] which was modified to take into account the

distribution of ε rather than assuming, as in Ref. 1, a fixed breakup

energy ε = 400 keV. The experimental ε distribution has been taken from

Morton et al.[9] for breakup energies $\varepsilon \leq$ 3 MeV; beyond this value of ε, the

shape of the distribution is not well known. Although this uncertainty may

introduce a potentially large error in the absolute efficiency and thus

in the absolute differential cross sections, the relative efficiencies

are estimated to be accurate to ± 10%. Figure 1(c) shows the energy

dependence of the calculated efficiency for the detection system.

The decay properties of a ^{2}He system with laboratory energy E and

relative energy ε impose certain restrictions on the lab energies E_1 and

E_2 of the two breakup protons p_1 and p_2. Momentum conservation demands

that, for given values of E and ε, neither of the single proton energies

E_1, E_2 be smaller than $E/2 - \sqrt{\varepsilon E}$ or larger than $E/2 + \sqrt{\varepsilon E}$. From this it

follows that $(E_1-E_2)^2/E \leq 4\varepsilon$ (with $E = E_1 + E_2$). This ratio was generated in

an analog device. An appropriate upper threshold was set on ε, which

resulted in some improvement of the observed peak to background ratio.

III. EXPERIMENTAL PROCEDURE

These experiments were performed using ^{4}He beams from the
Lawrence Berkeley Laboratory 88-inch Cyclotron. The choice of the beam
energy was mainly determined by the maximum energy range of the ^{2}He
detection system and the Q-values of the reactions. On the ^{24}Mg and ^{40}Ca
targets a bombarding energy of 55 MeV was utilized, whereas a 65 MeV beam
was used for all other targets. All solid targets were self-supporting.
For the gas targets, a 6 cm diameter cylindrical gas cell with a 2.11
mg/cm^2 Havar window was employed. Table I lists the isotopic purities
and thicknesses (or gas pressures) of the targets. The thicknesses of
the solid targets, determined from measurements of the energy losses of
α-particles from a ^{212}Pb source, are believed to be accurate to ± 10%.
For each target and angle, the maximum beam current was limited by the
electronic dead time of the detection system. Beam intensities ranged
from 15 nA at forward angles to 500 nA at backward angles. Typical
acquisition times for the spectra shown in this work were 2-3 hours.
On the average, approximately one ^{2}He event was recorded per 10^5 counts
in the ΔE detectors.

An energy resolution of 300-600 keV FWHM was obtained, determined
mainly by kinematic broadening due to the 4° horizontal acceptance angle
and the large dE/dθ for these light target nuclei. This led to ± 70 keV
uncertainties in establishing the excitation energies of the peaks
observed in the ^{2}He spectra. Unless indicated to the contrary, this
error is appropriate for the excitation energies determined for all
levels observed in the present study.

Typically the $(\alpha,{}^{2}\text{He})$ reaction was measured at four angles in the range $\Theta_{lab} = 12° - 35°$ for each target, in order to kinematically identify states and to discriminate against peaks arising from target contaminants. Detailed angular distributions over a wider angular range were measured for the ${}^{12}\text{C}$, ${}^{13}\text{C}$, ${}^{16}\text{O}$, and ${}^{28}\text{Si}$ targets. Apart from the potential error inherent in our efficiency calculations (see Sec. II), the quoted absolute differential cross sections are estimated to be accurate to within ± 20%.

IV. RESULTS AND DISCUSSION

It has been demonstrated in Ref. 1 that the $(\alpha, {}^2\text{He})$ reaction selectively populates levels that correspond to kinematically favored transitions in which the two transferred neutrons are simply captured in a singlet state about an undisturbed target core. At 65 MeV bombarding energy, the angular momentum mismatch for a surface reaction is about $(4-5)\hbar$ for 1p-shell targets and $(5-6)\hbar$ for 2s1d-shell targets. Because of this kinematic factor and the large overlap with the relative s motion of the neutron pair, states formed by capturing the two stripped neutrons coupled to $(d_{5/2})^2_4$ were observed to be strongly populated[1] in the reactions involving 1p-shell targets; on 2s1d-shell targets, configurations involving f-orbitals such as $(d_{3/2}f_{7/2})_5$ and $(f_{7/2})^2_6$ were expected to preferentially produced. Because of this difference in the particular high-spin states populated, this section will be divided into two parts. In Sec. IV A the $(\alpha, {}^2\text{He})$ reaction on the p-shell targets ${}^{12}\text{C}$, ${}^{13}\text{C}$, ${}^{14}\text{N}$, ${}^{15}\text{N}$, and ${}^{16}\text{O}$ will be discussed, and in Sec. IV B the results on the sd-shell targets ${}^{40}\text{Ca}$, ${}^{38}\text{Ar}$, ${}^{36}\text{Ar}$, ${}^{32}\text{S}$, ${}^{29}\text{Si}$, ${}^{28}\text{Si}$, ${}^{26}\text{Mg}$, ${}^{24}\text{Mg}$, ${}^{22}\text{Ne}$, ${}^{20}\text{Ne}$ and ${}^{18}\text{O}$ will be presented. (This order for Sec. IV B is taken to permit initial discussion of the $(f_{7/2})^2_6$ levels in a well-known region). In each part the observed energy spectra will be shown first, followed by a general discussion of the observed 2n states.

The results on the ${}^{12}\text{C}$, ${}^{13}\text{C}$, and ${}^{16}\text{O}$ targets have partially been presented in Ref. 1; however, given that the main emphasis in this report is on the systematics of 2n states of high spin over a wide range of nuclei, they are included here for completeness.

Because the intention of the present study has been to provide an initial survey of the properties of the $(\alpha, {}^2He)$ reaction, rather than to obtain and analyze detailed angular distributions, most J^π assignments made from our data must be considered highly probable rather than definitive.

A. The 1p-shell target nuclei.

1. $\underline{{}^{12}C(\alpha, {}^2He){}^{14}C}$ $(Q_o = -15.17 \text{ MeV})$

Figure 2 shows a spectrum of this reaction at $\Theta_{lab} = 12°$. Except for weak population of the ground state and a state at 14.9 ± 0.1 MeV, only the known 3^- state at 6.73 MeV and a state at 10.72 MeV are strongly populated. The 3^- state is known to be of dominant $(p_{1/2}d_{5/2})_3$ character[13], whereas recent studies of the 2n transfer reactions (t,p) (Ref. 14), $({}^{10}B, {}^8B)$ (Ref. 7) and $({}^{12}C, {}^{10}C)$ (Ref. 6) have established the $(d_{5/2})^2_4$ character of the state at 10.72 MeV. This excitation energy for the 4^+ state is in agreement with the previously reported values of 10.736 ± 0.005 MeV[14], and 10.77 ± 0.11 MeV[7]. It should be noted that the excitation energy of 10.55 MeV quoted in Ref. 1 for this 4^+ state is too low due to a non-linear behavior of the E-detectors used in that experiment. The state at 14.9 MeV in Fig. 2 was also observed with comparable relative strength in the study of the $({}^{10}B, {}^8B)$ reaction.[7]

2. $\underline{^{13}C(\alpha, {}^{2}He)^{15}C}$ $(Q_o = -18.90 \text{ MeV})$

A spectrum from this reaction at $\Theta_{lab} = 12°$ is shown in Fig. 3(a).

Since the ^{12}C and ^{13}C targets only differ by a $1p_{1/2}$ neutron, one expects

the $(\alpha, {}^{2}He)$ reaction on ^{13}C to populate preferentially states with the

same 2n-configurations observed in reactions on ^{12}C, but now coupled to

the $J^{\pi} = 1/2^-$ target core. Thus the states observed in the $^{12}C(\alpha, {}^{2}He)^{14}C$

spectra should be split (where possible) into two components in the

$^{13}C(\alpha, {}^{2}He)^{15}C$ spectra similar to the splitting observed in the analogous

(α, d) reactions on ^{12}C and ^{13}C.[2] Population of the doublet in ^{15}C observed

at 6.74 and 7.35 MeV can be interpreted as transitions to states having

predominantly $[\{^{12}C(0^+)p_{1/2}\}_{1/2} \otimes (d_{5/2})^2_4]_{7/2^-,9/2^-}$ character. As will

be shown later, the observed $L = 4$ behavior of the angular distributions

of the transitions to this doublet supports this assumption. The ratio of

the experimental differential cross sections, over the angular range

$\Theta_{lab} = 12°$ to $50°$, for the transitions to the states at 6.74 and 7.35 MeV is

about 4:5 which, applying the $(2J+1)$ rule for the relative population of

such states in stripping reactions, leads to the tentative assignments

of $J^{\pi} = 7/2^-$ for the 6.74 MeV state and $J^{\pi} = 9/2^-$ for the 7.35 MeV state.

This latter result corroborates the tentative assignment of $9/2^-$ for the

7.35 MeV state given in Ref. 15 (also see Sec. IV A4). Since the $5/2^+$

state at 0.74 MeV has a configuration $[\{^{12}C(0^+)p_{1/2}\}_{1/2} \otimes p_{1/2}d_{5/2}]_{5/2^-}$ the

$p_{1/2}$ neutron of ^{13}C and the transferred $p_{1/2}$ neutron must couple to $J = 0$

and no splitting can arise.

3. $\underline{^{14}N(\alpha,\,^{2}He)\,^{16}N}$ $(Q_{o} = -\,14.97\;\text{MeV})$

The $J^{\pi} = 1^{+}$, g.s. of ^{14}N can be described as $[^{12}C(0^{+})\nu p_{1/2}\pi p_{1/2}]_{1^{+}}$;

thus one expects that three states will be populated in the $^{14}N(\alpha,\,^{2}He)\,^{16}N$

reaction with configurations $[(^{14}N(g.s.,1^{+}) \otimes (d_{5/2})^{2}_{4}]_{J}$ and with $J = 3$, 4

or 5. The spectrum of this reaction shown in Fig. 3(b) appears to confirm

this expectation. The ^{16}N levels observed at 6.62 and 7.69 MeV (an unre-

solved doublet) contain the $L = 4$ strength which has split into three

components. Due to the poor energy resolution and the small splitting,

relative assignments of the $J^{\pi} = 3^{+}$, 4^{+}, 5^{+} components to the observed

peaks cannot be made. Transitions to the 2^{-}, g.s. of ^{16}N and the 3^{-}

state at 0.30 MeV, though unresolved, can be interpreted as populating the

configurations $[^{14}N(1^{+}) \otimes p_{1/2}\,d_{5/2}]_{2^{-},3^{-}}$, respectively. In addition

to these strongly populated states in ^{16}N, transitions to two states at

5.25 and 5.74 MeV are observed with moderate strength.

4. $\underline{^{15}N(\alpha,\,^{2}He)\,^{17}N}$ $(Q_{o} = -\,19.92\;\text{MeV})$

Since the neutron 1p-shell is full in ^{15}N, no p-orbits can be

populated with the $(\alpha,\,^{2}He)$ reaction on this target. Figure 4(a) shows a

spectrum from this reaction at $\Theta_{lab} = 13^{\circ}$. As can be seen, the only

states strongly populated are a doublet at 3.13 and 3.63 MeV. In the

simple picture which we are applying to the states populated by the

$(\alpha,\,^{2}He)$ reaction, the configuration of these states is expected to be

$[^{16}O(0^{+})p^{-1}_{1/2} \otimes (d_{5/2})^{2}_{4}]_{7/2^{-},9/2^{-}}$. In Ref. 16 the state at 3.13 MeV

has been assigned as $J^{\pi} = 7/2^{-}$ and the state at 3.63 MeV has been

tentatively assigned as $J^{\pi} = 9/2^-$. The (2J+1) rule applied to the

differential cross sections for the transitions to these states suggests

the same spin assignments. Furthermore, this agreement for states with

known spin and parity lends credence to the tentative $J^{\pi} = 7/2^-$ and $9/2^-$

assignments made for the 6.74 and 7.35 - MeV levels populated in the

$^{13}C(\alpha, ^2He)^{15}C$ reaction.

5. $\underline{^{16}O(\alpha, ^2He)^{18}O}$ $(Q_0 = - 16.11$ MeV)

Figure 4(b) shows a spectrum from this reaction at $\Theta_{lab} = 13°$.

The only strongly populated state in ^{18}O is the well known 4^+ state at

3.56 MeV. The $(d_{5/2})^2_4$ character of this state has been confirmed by shell-

model calculations[17,18] as well as by a recent study of the $^{16}O(^{10}B, ^8B)^{18}O$

reaction.[7] It is interesting to note that, although the 0^+, ground state and

the 2^+ state at 1.98 MeV in ^{18}O are also known to have $(d_{5/2})^2$

configurations, the cross sections for the transitions to these states in

the $(\alpha, ^2He)$ reaction are smaller by a factor of about 50 than that to the

4^+, 3.56 - MeV state due to the angular momentum mismatch, the angular

momentum coupling coefficents and the statistical weighting factor.

States with moderate strength are observed at 8.04, 9.15 and 10.3 MeV.

The overall resemblance between the ^{18}O spectrum and that from the

$^{18}O(\alpha, ^2He)^{20}O$ reaction (Sec. IV B11) suggests that corresponding transitions

involve similar transfers.

6. Discussion

The selectivity of the $(\alpha, {}^2He)$ reaction has been well demonstrated in the energy spectra shown in Secs. IV A1-5. The only states strongly populated in reactions on p-shell targets were those of $(p_{1/2}d_{5/2})_3$ and $(d_{5/2})^2_4$ character. Within the framework of this simple reaction mechanism, one might expect that the cross sections for populating 2n states above the core, i.e. the $(d_{5/2})^2_4$ states, should be mainly determined by the L-transfer and be almost independent of the mass number of the target.

Figure 5 presents differential cross sections for the transitions to the $(d_{5/2})^2_4$ configurations for the $(\alpha, {}^2He)$ reaction on the ${}^{12}C$, ${}^{13}C$, and ${}^{16}O$ targets. Since in the ${}^{13}C(\alpha, {}^2He){}^{15}C$ reaction the $(d_{5/2})^2_4$ strength is split, the sum of the two components is shown. The dashed line represents an experimental L = 4 distribution obtained from a least squares fit to the ${}^{14}C$, 4^+ transition. As can be seen, all distributions have the same shape and magnitude. Only a few angles have been measured for the $(\alpha, {}^2He)$ reaction on the ${}^{14}N$ and ${}^{15}N$ targets, but again the sum of the differential cross sections at those angles for the $(d_{5/2})^2_4$ transitions to states in ${}^{16}N$ and ${}^{17}N$ are the same as for those shown in Fig. 5.

The $(\alpha, {}^2He)$ cross sections are about 50 times smaller than those of the (α, d) reaction on the same target at similar incident energies. This is comparable to the difference observed between 2n and np transfer in heavy-ion reactions,[6] indicating again that the same mechanism is involved in the (α, d) and $(\alpha, {}^2He)$ reactions. This is also confirmed in a recent study of the ${}^{28}Si(\alpha, {}^2He){}^{30}Si$ reaction by de Meijer et al.[19], who obtained reasonable fits to the ${}^2He$ angular distributions using zero-range DWBA with optical model parameters that fit their ${}^{28}Si(\alpha, d){}^{30}P$ data.

B.   The 2s1d-shell target nuclei

1. $\underline{^{40}Ca(\alpha,{}^{2}He)^{42}Ca}$ (Q_o = -8.46 MeV)
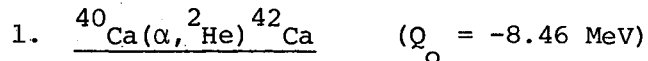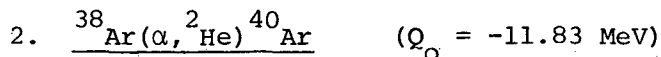
Figure 6(a) presents a spectrum from this reaction at Θ_{lab} = 15°.
The only strongly populated peak corresponds to transitions to the 6^{+},
3.19 MeV-state in ^{42}Ca. This state is known to be a 2n state of $(f_{7/2})^2_6$
character.[18] Transitions to the other members of the $(f_{7/2})^2$, T = 1
multiplet with J^{π} = 0^{+}, 2^{+}, and 4^{+} at 0., 1.52 and 2.75 MeV, respectively,
were also observed, but with a reduced cross section. Since simple
shell-model calculations (see Sec. V) predict a state with an $(f_{7/2}f_{5/2})_6$
configuration at 7.23 MeV in ^{42}Ca, the state observed at 7.40 MeV is a
candidate for such a state.

2. $\underline{^{38}Ar(\alpha,{}^{2}He)^{40}Ar}$ (Q_o = -11.83 MeV)

Since ^{38}Ar has the same closed shell neutron configuration as ^{40}Ca,
the spectra of the $(\alpha,{}^{2}He)$ reaction on this target should be very similar
to those observed on the ^{40}Ca target, as is demonstrated in Fig. 6(b). The
excitation energies as well as the observed relative strengths of the
transitions to the J^{π} = 6^{+}, 4^{+}, 2^{+}, 0^{+} members of the $(f_{7/2})^2$ multiplet
are almost identical to those observed in the $^{40}Ca(\alpha,{}^{2}He)^{42}Ca$ reaction.
The 3.47-MeV level in ^{40}Ar has previously been observed in a study of the
$^{38}Ar(t,p)^{40}Ar$ reaction[20] where a tentative J^{π} = 6^{+} assignment has been made.
Certainly the analogous ^{42}Ca and ^{40}Ar spectra observed in the present study
help establish such an assignment. The state observed at 9.0 ± 0.1 MeV and
the broad state (or unresolved states) between 7.5 and 9.0 MeV in ^{40}Ar
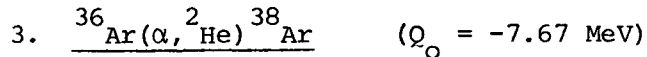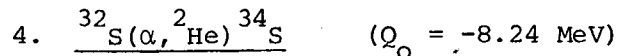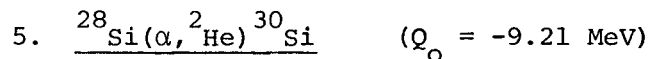probably correspond to the states observed in ^{42}Ca at 7.40 and 9.04 MeV,
respectively.

3. $\underline{^{36}Ar(\alpha,^2He)^{38}Ar}$ (Q_o = -7.67 MeV)

Figure 7 shows a spectrum from this reaction at Θ_{lab} = 13°. All

observed peaks below 7.5 MeV could be identified with known states of

^{38}Ar (Ref. 21). Again, the transition to the 6$^+$ state has the largest

cross section. Although the J^π = 6$^+$ assignment of the 6.41-MeV state has

recently been established in a study of the $^{24}Mg(^{16}O,2p\gamma)$ reaction[22], the

present experiment confirms its $(f_{7/2})^2_6$ character. The 5$^-$ states at

4.59 and 5.66 MeV are of dominant $(d_{3/2}f_{7/2})_5$ character.[23] This splitting

of the 5$^-$ strength in ^{38}Ar has been successfully described by the shell-

model calculations of Engelbertink and Glaudemans.[23] The states observed

at higher excitation energies could not definitely be identified as ^{38}Ar

states. Their slightly different kinematic behavior indicates that they

might originate from an unidentified target contaminant.

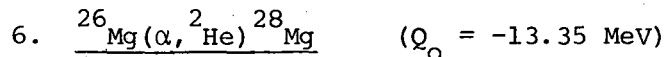4. $\underline{^{32}S(\alpha,^2He)^{34}S}$ (Q_o = -8.24 MeV)

A spectrum from this reaction on an Sb_2S_3 target is presented in

Fig. 8. The known[24] 5$^-$ state at 5.69 MeV and a previously unknown state

in ^{34}S at 8.45 MeV are preferentially populated. Furthermore, the known

3$^-$ state at 4.62 MeV and two previously unknown states at 7.24 and 10.7 ±

0.1 MeV are populated with moderate strength. The peaks seen at higher

excitation energies could not definitely be identified as transitions to

^{34}S levels.

The 5$^-$ state in ^{34}S is known to be of predominant $(d_{3/2}f_{7/2})$

character, since the (d,p) reaction on ^{33}S (which, in its ground state,

has a $[^{32}S(0^+) \otimes \nu d_{3/2}]_{3/2^+}$ configuration) shows a strong ℓ = 3
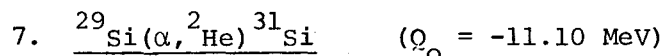
transfer to the 5.69 MeV state.[24]   The state at 8.45 MeV is most likely of

$(f_{7/2})_6^2$ character which is in agreement with simple shell-model calculations

(see Sec. V).   It should be noted that, in a study of the $^{32}S(t,p)^{34}S$ reaction,[25]

the J^{π} = 4^+, 2^+, and 0^+ members of the $(f_{7/2})^2$ multiplet were identified at

8.42, 7.80 and 5.86 MeV, respectively, though the 6^+ member was not observed.

Simple shell-model calculations (see Sec. V) indicate that the state observed

at 10.7 MeV could be of $(f_{7/2}f_{5/2})_6$ character, but no definite assignment

can be made based on this limited survey.

5. $\underline{^{28}Si(\alpha, {}^2He)^{30}Si}$ (Q_o = -9.21 MeV)

A spectrum from the $(\alpha, {}^2He)$ reaction at θ_{lab} = 12° on this closed

$d_{5/2}$ subshell target nucleus is shown in Fig. 9(a).   The known[24] 3^- and 5^-

states at 5.49 and 7.04 MeV, respectively, and two states at 8.95 and 10.67

MeV are substantially populated.   Recently, de Meijer et al.[19] published

a study of this reaction at E_{α} = 65 MeV, and our excitation energies

and differential cross sections for the observed levels agree with their

values within errors.   They obtained detailed angular distributions for

the $^{28}Si(\alpha, {}^2He)^{30}Si$ reaction which were analyzed with DWBA calculations,

using optical model parameters from (α,d) data analysis and taking deuteron

parameters for ^2He.   Their analysis established that the ^{30}Si levels at

5.49, 7.04, 8.95 and 10.67 MeV possess 2n configurations of $(2s_{1/2}f_{7/2})_3$

$(d_{3/2}f_{7/2})_5$, $(f_{7/2})_6^2$, and $(f_{7/2}f_{5/2})_6$ character, respectively.   The

presence of an $(f_{7/2}f_{5/2})_6$ configuration so close to the $(f_{7/2})_6^2$ configuration

in ^{30}Si is somewhat surprising, but can be explained by the fact that the

experimental $f_{7/2}$ - $f_{5/2}$ single particle states in ^{29}Si are only separated

by 2.57 MeV, whereas typically those two single particle energies differ by

about 3-4 MeV throughout the rest of the sd-shell.[24]

6. <u>$^{26}Mg(\alpha, ^2He)^{28}Mg$</u> $(Q_0 = -13.35 \text{ MeV})$

Since ^{26}Mg has the same closed $d_{5/2}$ - subshell neutron configuration as ^{28}Si, the $(\alpha, ^2He)$ spectra on these two targets are expected to be very similar. Comparing Figs. 9(a) and (b) confirms this expectation. The states observed at 6.46, 8.88 and 9.78 MeV were previously unknown. In analogy with the population of known states in ^{30}Si, these states can be preliminarily assigned as being of $(d_{3/2}f_{7/2})_5$, $(f_{7/2})^2_6$ and $(f_{7/2}f_{5/2})_6$ character, respectively.

7. <u>$^{29}Si(\alpha, ^2He)^{31}Si$</u> $(Q_0 = -11.10 \text{ MeV})$

In its ground state, ^{29}Si can be described as $(^{28}Si(0^+) \otimes 2s_{1/2})_{1/2}^+$ and thus one can expect the $(\alpha, ^2He)$ reaction on ^{29}Si to populate the same 2n states as on a ^{28}Si(or ^{26}Mg) target, coupled to the $2s_{1/2}$ neutron. A spectrum of the $^{29}Si(\alpha, ^2He)^{31}Si$ reaction is shown in Fig. 10. Three previously unknown states in ^{31}Si at 5.00, 5.41 and 8.27 MeV are preferentially populated. The doublet at 5.00 and 5.41 MeV most probably arises from the coupling of the $(d_{3/2}f_{7/2})_5$ configuration to the $s_{1/2}$ neutron of the ^{29}Si core, so that these two states presumably have J^π assignments of $9/2^-$ and $11/2^-$. An assignment via the simple (2J+1) dependence of the cross section (see Secs. IV A2 and IV A4) could not be made, since at most angles this doublet is unresolved. The state at 8.27 MeV can possibly be explained as an unresolved doublet of either

$$[\{^{28}Si(0^+)2s_{1/2}\}_{1/2} \otimes (f_{7/2})^2_6]_{11/2^+, 13/2^+} \quad \text{or}$$

$$[\{^{28}Si(0^+)2s_{1/2}\}_{1/2} \otimes (f_{7/2}f_{5/2})_6]_{11/2^+, 13/2^+} \quad \text{configuration;}$$

the separation in energy of the 8.27 MeV-states relative to the centroid

of the 5.00 and 5.41 MeV states, when compared to the spectra from the

$(\alpha, {}^2\mathrm{He})$ reaction on ${}^{28}\mathrm{Si}$ and ${}^{26}\mathrm{Mg}$, leads to a preference for the latter
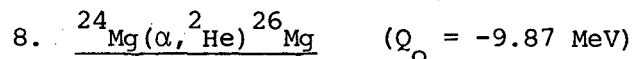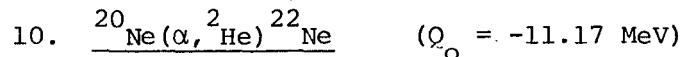
configuration.

$$8. \quad \underline{{}^{24}\mathrm{Mg}(\alpha, {}^2\mathrm{He}){}^{26}\mathrm{Mg}} \quad (Q_0 = -9.87 \text{ MeV})$$

Figure 11(a) presents a spectrum from this reaction at $\Theta_{\mathrm{lab}} = 12°$.

Besides moderate population of the known 4^+ state^{24} at 5.47 MeV, two

previously unknown states at 8.62 and 11.23 MeV are strongly populated.

From the systematics discussed in Sec. V it follows that these two states

are presumably populated by $(d_{3/2}f_{7/2})_5$ and $(f_{7/2})^2_6$ transitions, respectively.

$$9. \quad \underline{{}^{22}\mathrm{Ne}(\alpha, {}^2\mathrm{He}){}^{24}\mathrm{Ne}} \quad (Q_0 = -14.23 \text{ MeV})$$

Figure 11(b) shows a spectrum from this reaction at $\Theta_{\mathrm{lab}} = 13°$.

All states observed above the 2^+, 3.87-MeV level were previously unknown.

${}^{24}\mathrm{Ne}$ states at 6.36 and 8.15 MeV and a broad level at 11.35 ± 0.15 MeV are

strongly populated. In addition, a state at 9.88 MeV is observed with

moderate strength. Although ${}^{22}\mathrm{Ne}$ has the same neutron configuration as

${}^{24}\mathrm{Mg}$, the spectra of the final nuclei ${}^{24}\mathrm{Ne}$ and ${}^{26}\mathrm{Mg}$ are not as similar as has

been previously observed in populating the pairs of isotones ${}^{28}\mathrm{Mg}$ vs.

${}^{30}\mathrm{Si}$ or ${}^{40}\mathrm{Ar}$ vs. ${}^{42}\mathrm{Ca}$. This can perhaps be related to the fact that,

unlike the ${}^{26}\mathrm{Mg}$, ${}^{28}\mathrm{Si}$, ${}^{38}\mathrm{Ar}$, and ${}^{40}\mathrm{Ca}$ targets, those of ${}^{22}\mathrm{Ne}$

and ${}^{24}\mathrm{Mg}$ do not have closed neutron shells or subshells. As will

be shown from the systematics (Sec. V), the state at 8.15 MeV in

^{24}Ne is probably of $(d_{3/2}f_{7/2})_5$ character and the broad state

at 11.35 MeV is possibly of $(f_{7/2})_6$ character, with the latter sug-

gestion being quite tentative. The state at 6.36 MeV cannot be assigned

in the present study; it is either the counterpart of the 5.47 MeV-state in

^{26}Mg or of $(s_{1/2}f_{7/2})_3$ character. In the latter case the absence of an

analogous peak in the ^{26}Mg spectrum is puzzling.

10. $\underline{^{20}Ne(\alpha, {}^2He)^{22}Ne}$ $(Q_0 = -11.17$ MeV$)$

A spectrum from this reaction at $\Theta_{lab} = 12.5°$ is shown in Fig. 12(a).

In addition to the relatively strong population of a doublet at 9.16 and

9.44 MeV, many states are populated with moderate strength in this reaction.

The systematics of the 2n states, as discussed in Sec. V, indicates that

one of the states of the doublet is likely to be of $(d_{3/2}f_{7/2})_5$ character,

but a definite assignment is not justified.

11. $\underline{^{18}O(\alpha, {}^2He)^{20}O}$ $(Q_0 = -16.74$ MeV$)$

A spectrum from this reaction is shown in Fig. 12(b). In addition

to the transitions to the known 0^+, 2^+ and 4^+ states[26] at 0., 1.67 and

3.57 MeV, respectively, previously unknown states at 7.78, 8.78 and

10.2 ± 0.1 MeV are populated in ^{20}O. Although configurations of $(d_{5/2}d_{3/2})_4$

and $(d_{3/2}f_{7/2})_5$ are expected in this high excitation region, no assignments

can be made in this limited survey. Although ^{20}O has the same neutron

configuration as ^{22}Ne, the spectra from the $(\alpha, {}^2He)$ reaction populating

these nuclei again lack the pronounced similarities observed in reactions

producing isotones higher in the sd-shell (see also Sec. IV B9).

12. Discussion

As already pointed out in Section IV A6, our simple model of the $(\alpha, {}^2\text{He})$ reaction leads one to expect that cross sections for transitions to the strongly populated 2n states should, for given configurations, be largely independent of the target nucleus, so long as the target does not contain any such nucleons. Table II presents the differential cross sections for transitions on such targets to the observed states with $(d_{3/2}f_{7/2})_5$ and $(f_{7/2})^2_6$ character at $\Theta_{lab} = 15°$. It can be seen that for reactions over a wide range of target nuclei, the experimental cross sections, in general, are quite similar. For $(d_{3/2}f_{7/2})_5$ and $(f_{7/2})^2_6$ transitions, the average cross sections at this angle are about 60 and 40 μb/sr, respectively. This consistency of the cross sections indicates again the simple mechanism of the $(\alpha, {}^2\text{He})$ reaction.

V. SHELL-MODEL CALCULATIONS AND SYSTEMATICS

Predicated on the observed selectivity of the $(\alpha, {}^{2}\text{He})$ reaction,
simple shell-model calculations have been carried out in order to interpret
further the character of the strongly populated states. The $T_z = 0$ target
nuclei from ${}^{24}\text{Mg}$ to ${}^{40}\text{Ca}$ were each assumed to be an inert core and the two
neutrons were allowed to occupy the valence orbits in the 2s1d and
1f2p shells.

The single-particle energies ε_j were taken to be the separation
energies of the single particle levels in the $A_{core} +1$ nucleus:

$$\varepsilon_j = E(A+1, J=j) - E(A) \tag{1}$$

where $A = A_{core}$. From the dominant appropriate ℓ-transfers in single-
nucleon transfer reactions,[24] the locations of the single particle levels
were determined. Table III gives a list of the single particle energies
utilized. The excitation energy of the 2n states was calculated
according to

$$E_x(A+2, \; j_1 j_2 J) = \varepsilon_{j_1} + \varepsilon_{j_2} + \langle j_1 j_2 |v| j_1 j_2 \rangle_J + B_{2n}(A+2, \text{g.s.}), \tag{2}$$

where B_{2n} and $\langle j_1 j_2 |v| j_1 j_2 \rangle_J$ are the 2n binding energy and the
two-body matrix element (TBME), respectively. The calculated TBME's of Kuo and
Brown[27] have been applied except for the $(d_{3/2} f_{7/2})_{3,5}$ cases, where the values
empirically evaluated by Erné[28] have been used, since they give much
better fits to the known $J^\pi = 3^-$ and 5^- states. Those TBME's not listed by
Kuo and Brown have been calculated from the modified surface delta inter-
action with the A = 37, 39 parameters listed in Ref. 29.

When several configurations yielded states with the same spin J, the configuration interaction was taken into account by diagonalizing the Hamiltonian matrix

$$H_{\alpha\beta} = (\epsilon_{j_{1\alpha}} + \epsilon_{j_{2\alpha}})\delta_{\alpha\beta} + <j_{1\alpha}j_{2\alpha}|V|j_{1\beta}j_{2\beta}>_J + B_{2n}(A+2,g.s.)\delta_{\alpha\beta} . \quad (3)$$

Due to the difference in single particle energies, there usually is a large gap in the energy between the second and the higher pure configurations. For this reason, in the present calculations these higher configurations were neglected, which reduced the calculation of the energy levels to simple 2 × 2 matrix diagonalizations.

Figure 13 compares the calculations for ^{30}Si, ^{34}S and ^{42}Ca with the energy spectra observed in the present study. Except for the energies of the ground states, which are very sensitive to the limitations of the present approach, the calculations are in good agreement with experiment, especially so for the ^{30}Si nucleus, and are additional support for the assignments suggested in the previous sections. The calculated excitation energies for the $J^{\pi} = 5^-$ and 6^+ states in ^{26}Mg, ^{30}Si, ^{34}S, ^{38}Ar and ^{42}Ca are listed in Table IV.

Another shell-model approach is given in the Bansal-French (BF) weak-coupling method[30-33] for computing the energies of particle-hole states. In studies of the (α,d) reaction on many sd-shell nuclei[2-5], a linear dependence of the binding energy B_{np} of the neutron-proton pair in the observed $(f_{7/2})^2_7$ states versus the mass number of the final nucleus has been observed and successfully explained by the BF method. This method will be discussed below and the binding energies of the 2n states will be calculated and compared with the experimental data.

The total energy of a nucleus $A_0 + p\text{-}h$ with p particles and h holes relative to a closed shell nucleus A_0 is given by:

$$E(A_0 + p\text{-}h) = E(A_0) + E(p) - E(h) + \langle ph | V_{ph} | ph \rangle , \tag{4}$$

where $E(p)$ and $E(h)$ are the energies of p particles and h holes relative to $E(A_0)$. In the model of Bansal and French, a weak interaction is assumed between the particles and holes such that the values of $E(p)$ and $E(h)$, which include the interactions of the particles and holes among themselves, can be obtained empirically from the binding energies of the nuclei A_0, $A_0 + p$ and $A_0 - h$ by

$$E(p) = E(A_0 + p) - E(A_0) \tag{5}$$

$$E(h) = E(A_0) - E(A_0 - h) . \tag{6}$$

In Eq. (4) the last term represents the interaction energy between the particles and the holes which was assumed by Bansal and French to be of the following form:

$$\langle ph | V_{ph} | ph \rangle = -p \cdot h \cdot a + b \, \vec{t}_p \cdot \vec{t}_h , \tag{7}$$

where a is the two-body matrix element $\langle j_p j_h^{-1} | V_{ph} | j_p j_h^{-1} \rangle_{JT}$ averaged over all allowed values of J and T, and b is the separation of the center of gravity of the T=0 and T=1 states.

By inserting Eqs. (5)-(7) in Eq. (4), one obtains for the energy of the nucleus $A = A_0 + p\text{-}h$

$$E(A,T,T_z) = E(A_0 + p, T_p, T_{zp}) + E(A_0 - h, T_h, T_{zh}) - E(A_0, 0, 0)$$
$$- p \cdot h \cdot a + b \frac{1}{2} \left[T(T+1) - T_p(T_p+1) - T_h(T_h+1) \right] + \varepsilon_c , \tag{8}$$

where ε_c is the Coulomb interaction energy between the particles and the holes, which was not included in V_{ph}.

The two-neutron binding energy B_{2n} of states with dominant $(f_{7/2})^2$

character in a nucleus A near the closed shell nucleus ^{40}Ca can readily be

obtained from Eq.(8) using $E(A_0) = E(^{40}Ca\ g.s.)$, $E(A_0+p) = E(^{42}Ca(f_{7/2})^2)$

$E(A_0-h) = E(A-2,\ g.s.\ 0^+)$, $p = 2$, $h = 40-(A-2)$, and $\varepsilon_c = 0$, one then finds:

$$B_{2n}(A(f_{7/2})^2_6) = B_{2n}(^{42}Ca(f_{7/2})^2_6) + 2\cdot(42-A)\cdot a - b\cdot(T-1) \qquad (9)$$

$$B_{2n}(A(f_{7/2})^2_0) = B_{2n}(^{42}Ca(f_{7/2})^2_0) + 2\cdot(42-A)\cdot a - b\cdot(T-1) \qquad (10)$$

In a similar fashion, both B_{2n} for states with $(d_{3/2}f_{7/2})_5$ character as well as

the one-neutron binding energy B_n of $f_{7/2}$ single-particle states can be

derived:

$$B_{2n}(A(d_{3/2}f_{7/2})_5) = B_{2n}(^{34}S(d_{3/2}f_{7/2})_5) + 2\cdot(34-A)\cdot a - b\cdot(T-1) \qquad (11)$$

$$B_n(A\ f_{7/2}) = B_n(^{41}Ca\ f_{7/2}) + 1\cdot(41-A)\cdot a \qquad (12)$$

In Fig. 14 the experimental B_{2n} values of the $(f_{7/2})^2_6$ and $(d_{3/2}f_{7/2})_5$ states from

the present study are plotted versus A of the final nucleus. In addition,

the experimental B_{2n} values[29] of states with the $(f_{7/2})^2_0$ configuration as well as

the B_n values[29] of $f_{7/2}$ single-neutron states relative to $J^\pi = 0^+$ nuclei are

also indicated in Fig. 14. The solid lines represent B_{2n} and B_n calculated

(Eqs. (9)-(12)) using the common values $a = -0.30$ MeV and $b = 2.6$ MeV.

The observed linear dependence of B_{2n} on A is well reproduced by the

BF model. This indicates that a is essentially independent of A, as assumed

in Eqs. (9)-(12). As Sherr et al.[32] pointed out, this fact is remarkable and

somewhat surprising, since a contains different particle-hole interactions

depending on A. For the $(f_{7/2})^2$ states, for instance, in the case of ^{38}Ar

a contains only $(f_{7/2}d_{3/2}^{-1})$ interactions, whereas in ^{26}Mg in addition the $(f_{7/2}s_{1/2}^{-1})$

and $(f_{7/2}d_{5/2}^{-1})$ interactions are included. Although it is known[27] that these

interaction energies differ substantially from one another, the averaging is

believed to smooth out any differences.

The fact that the same a parameter fits the states with $(f_{7/2})^2_0$ and $(f_{7/2})^2_6$ configurations is expected in the BF model, since they involve the same particle-hole interactions. The differences in energy of these two states is a result of the particle-particle interaction, which is included in $E(p)$, (Eq. (5)), and which does not affect the particle-hole interaction. On the other hand, one would expect that the value of a would differ for the $(f_{7/2})^2$ states vs. the $(d_{3/2}f_{7/2})$ states, since the latter also involve interactions of a $d_{3/2}$ particle with the various holes. The fact that the same value of a fits both configurations could be fortuitous or could be again the result of averaging. It is interesting to note that this value for a of -0.30 MeV has also been found in a similar analysis[32] of the binding energies B_{np} of neutron-proton states with $(f_{7/2})^2$ character. Sherr et al.[32] also obtained $b = 2.88$ MeV which compares well with our value of $b = 2.60$ MeV. These values are in good agreement with those of Bansal and French[30] and Zamick[31] who found $a = -0.25$ MeV, $b = 2.9$ MeV and $a = -0.30$ MeV, $b = 2.90$ MeV, respectively, for nuclei in the region of ^{40}Ca.

The good agreement between the calculated and the experimental excitation energies for the $J^{\pi} = 5^-$ and 6^+ states in the simple shell model calculations also means that this approach gives B_{2n} values which are linearly dependent on A. This indicates similarities in both methods in the calculation of the B_{2n}. In the simple shell model approach the two-neutron binding energy is given merely by the sum of the single particle separation energies plus the TBME, which is independent of A (here we ignore the contribution from configuration mixing). Thus all A dependence in B_{2n} is related to the A dependence of the single-particle separation energies. A linear dependence of the B_{2n} values, therefore, can be expected if the single-particle separation energies are

linearly dependent on A. As is shown in Fig. 14, the $f_{7/2}$ single-particle

separation energies indeed show a linear dependence on A. The fact that

the slope for the $(f_{7/2})^2$ states is twice that of the $f_{7/2}$ states follows

clearly from this reasoning.

Looking at Eq. (9), (10) and (12) one sees that B_{2n} can be

expressed as $B_{2n} = C_1 + C_2 \cdot A$ for a group of states with the same T.

Similarly $B_n = C_3 + \frac{1}{2} C_2 \cdot A$ since in this case the number of particles

involved is half that in the two-neutron case. Thus the success of

the Bansal-French method depends on the linear correspondence of the single-

neutron separation energies with A too. This also implies that in both methods

the slope for the $(d_{3/2} f_{7/2})_5$ lines (Fig. 14) should be the same as for the

$(f_{7/2})^2$ lines if the difference in the $\varepsilon_{d_{3/2}} - \varepsilon_{f_{7/2}}$ single nucleon

separation energy, $\Delta\varepsilon$, remains constant. Indeed, the variation in these

values for $\Delta\varepsilon$ of 2.99, 2.35 and 2.93 MeV for A = 25, 29 and 33 respectively,

is too small to affect the slope.

It is interesting to note that calculations of $f_{7/2}$ separation

energies in a Woods-Saxon well with parameters of Ref. 33 (V = 51 MeV,

r_0 = 1.27 fm, a = 0.65 fm and $V_{s.o.}$ = 16.4 MeV) yield more or less a linear

A-dependence too, but the slope differs from the one observed here by a

factor of two.

VI. SUMMARY

The $(\alpha, {}^{2}\text{He})$ reaction has been investigated over a wide range of

1p- and 2s1d-shell targets with results which demonstrate a pronounced

selectivity in this reaction for populating two-neutron states of high spin.

On 1p-shell targets, preferential transitions to states of $(p_{1/2}d_{5/2})_{3}$ and

$(d_{5/2})^{2}_{4}$ character have been observed; on 2s1d-shell targets, states

with $(d_{3/2}f_{7/2})_{5}$ and $(f_{7/2})^{2}_{6}$ configurations were selectively populated,

many of which were previously unknown.

The excitation energies of some of the known and assumed 5^{-} and 6^{+}

states could be understood in terms of a simple shell model calculation

describing the states as a core plus two neutrons and taking the separation

energy for the neutron as the single-particle energy. As was earlier observed[2-5]

in the (α, d) reaction on 2s1d-shell nuclei, the two-neutron binding energies

displayed a linear dependence on the mass number which could be reproduced

by a calculation employing the Bansal-French[30-33] method. The parameters

a and b entering the calculation turned out to be very similar to the ones

obtained in the (α, d) work.[32] The success of the Bansal-French method applied to

these nuclei seems to be related to the linear A-dependence of the neutron

separation energy.

It would appear from the present results that extensions of this

approach to provide detailed investigations of neutron-rich product nuclei could

be quite valuable; indeed, a comprehensive study of two-neutron transfer via the

${}^{28}\text{Si}(\alpha, {}^{2}\text{He}){}^{30}\text{Si}$ reaction has already been reported[19].

V.   ACKNOWLEDGEMENTS

REFERENCES AND FOOTNOTES

[+]Present address: Institut für Strahlen- und Kernphysik der Universität Bonn,

Nussallee 14-16, 53 Bonn, West Germany.

[++]On leave from: Kernfysisch Versneller Instituut, University of Groningen,

Groningen 8002, The Netherlands.

1. R. Jahn, G. J. Wozniak, D. P. Stahel, and J. Cerny, Phys. Rev. Lett.

    $\underline{37}$, 812 (1976).

2. E. Rivet, R. H. Pehl, J. Cerny, and B. G. Harvey, Phys. Rev. $\underline{141}$, 1021 (1966).

3. C. C. Lu, M. S. Zisman, and B. G. Harvey, Phys. Rev. $\underline{186}$, 1086 (1969).

4. H. Nann, W. S. Chien, A. Saha, and B. H. Wildenthal, Phys. Lett. $\underline{60B}$, 32 (1975).

5. R. M. Del Vecchio, R. T. Kouzes, and R. Sherr, Nucl. Phys. $\underline{A265}$, 220 (1976).

6. N. Anyas-Weiss et al., Phys. Rep. $\underline{12C}$, 201 (1974).

7. M. Hamm and K. Nagatani, Phys. Rev. C (to be published).

8. G. J. Wozniak, N. A. Jelley, and J. Cerny, Nucl. Instrum. Methods $\underline{120}$, 29 (1974).

9. B. J. Morton, E. E. Gross, E. V. Hungerford, J. J. Malanify, and A. Zucker,

    Phys. Rev. $\underline{169}$, 825 (1968).

10. K. M. Watson, Phys. Rev. $\underline{88}$, 1163 (1952).

11. A. E. Migdal, Soviet Phys. JETP $\underline{1}$, 2 (1955).

12. The program is available from the authors.

13. W. W. True, Phys. Rev. $\underline{130}$, 1530 (1963).

14. S. Mordechai et al., to be published.

15. F. Ajzenberg-Selove, Nucl. Phys. $\underline{A268}$, 1 (1976).

16. F. Ajzenberg-Selove, Nucl. Phys. $\underline{A281}$, 1 (1977).

17. T. T. S. Kuo and G. E. Brown, Nucl. Phys. $\underline{85}$, 40 (1966).

18. I. Kanestrøm and H. Koren, Nucl. Phys. A130, 527 (1969).

19. R. J. de Meijer, R. Kamermans, J. van Driel and H. P. Morsch,

    Phys. Rev. C 16, 2442 (1977).

20. E. R. Flynn, O. Hansen, R. F. Casten, J. D. Garrett, and F. Ajzenberg-Selove,

    Nucl. Phys. A246, 117 (1975).

21. J. J. Kolata, J. W. Olness, E. K. Warburton, and A. R. Poletti,

    Phys. Rev. C 13, 1944 (1976).

22. M. A. van Driel, H. H. Eggenhuisen, G. A. P. Engelbertink, L. P. Ekström,

    and J. A. J. Hermans, Nucl. Phys. A272, 466 (1976).

23. G. A. P. Engelbertink and P. W. M. Glaudemans, Nucl. Phys. A123, 225 (1969).

24. P. M. Endt and C. van der Leun, Nucl. Phys. A214, 1 (1972).

25. D. J. Crozier, H. T. Fortune, R. Middleton, and S. Hinds, Phys. Lett.

    46B, 189 (1973).

26. F. Ajzenberg-Selove, Nucl. Phys. A190, 1 (1972).

27. T. T. S. Kuo and G. E. Brown, Nucl. Phys. A114, 241 (1968).

28. F. C. Erné, Nucl. Phys. 84, 91 (1966).

29. S. Maripuu and G. A. Hokken, Nucl. Phys. A141, 481 (1970).

30. R. K. Bansal and J. B. French, Phys. Lett. 11, 145 (1964).

31. L. Zamick, Phys. Lett. 19, 580 (1965).

32. R. Sherr, R. Kouzes, and R. Del Vecchio, Phys. Lett. 52B, 401 (1974).

33. G. F. Bertsch, The Practitioner's Shell Model, (North-Holland Publishing

    Company, Amsterdam 1972) p. 86.

Table II. Excitation energies and cross sections for $(d_{3/2}f_{7/2})_{5^-}$ and $(f_{7/2})^2_{6^+}$ states observed in the $(\alpha,{}^2He)$ reactions.

Final Nucleus	Beam Energy (MeV)	$(d_{3/2}f_{7/2})_{5^-}$		$(f_{7/2})^2_{6^+}$	
		E_x (MeV)	$\frac{d\sigma}{d\Omega}$ (15° lab) (μb/sr)	E_x (MeV)	$\frac{d\sigma}{d\Omega}$ (15° lab) (μb/sr)
${}^{24}Ne$	65	8.15	25	11.35	30
${}^{26}Mg$	55	8.62	60	11.23	25
${}^{28}Mg$	65	6.46	40	8.88	30
${}^{30}Si$	65	7.04	65	8.95	50
${}^{34}S$	65	5.69	100	8.45	85
${}^{38}Ar$	65			6.41	35
${}^{40}Ar$	65			3.47	30
${}^{42}Ca$	55			3.19	40

Table III.   Single particle energies (in MeV) used in the shell-model calculations.

A_{core}	$1d_{5/2}$	$2s_{1/2}$	$1d_{3/2}$	$1f_{7/2}$	$2p_{3/2}$	$1f_{5/2}$
^{24}Mg	-7.332	-6.747	-6.357	-3.364	-3.918	
^{28}Si		-8.474	-7.201	-4.850	-3.540	-2.283
^{32}S			-8.643	-5.709	-5.423	-1.954
^{36}Ar			-8.789	-7.178	-6.299	-4.384
^{40}Ca				-8.363	-6.420	-3.481

Table IV.   Excitation and two-neutron binding energies (in MeV) and main configurations of $J^\pi = 5^-$ and 6^+ states resulting from the shell model calculations.

$A_{core}+2$	$J^\pi=5^-$ $(d_{5/2}f_{7/2})$		$(d_{3/2}f_{7/2})$		$J^\pi=6^+$ $(f_{7/2})^2$		$(f_{7/2}f_{5/2})$	
	E_x	B_{2n}	E_x	B_{2n}	E_x	B_{2n}	E_x	B_{2n}
^{26}Mg	7.67	10.75	9.21	9.22				
^{30}Si			7.46	11.62	9.32	9.77	11.35	7.73
^{34}S			6.14	13.92	8.69	11.37	11.68	8.38
^{38}Ar			5.09	15.54	6.23	14.39	8.44	12.19
^{42}Ca					3.27	16.63	7.23	12.60

FIGURE CAPTIONS

Fig. 1. a) Schematic diagram of the ^{2}He detection system.

b) A gated time-of-flight difference spectrum between events in the two telescopes.

c) The detection efficiency as a function of the ^{2}He energy.

Fig. 2. A spectrum of the ^{12}C(α,^{2}He)^{14}C reaction at E_α = 65 MeV and Θ_{lab} = 12°.

Fig. 3. Spectra of the (α,^{2}He) reaction at E_α = 65 MeV on

a) ^{13}C at Θ_{lab} = 12° and b) ^{14}N at Θ_{lab} = 13°.

Fig. 4. Spectra of the (α,^{2}He) reaction at E_α = 65 MeV and Θ_{lab} = 13° on

a) ^{15}N and b) ^{16}O.

Fig. 5. A comparison of some L = 4 (α,^{2}He) angular distributions.

The dashed curve represents the interpolated experimental angular distribution for the transition to the 10.72-MeV, 4$^+$ state in ^{14}C.

Fig. 6. Spectra of the (α,^{2}He) reaction on:

a) ^{40}Ca at E_α = 55 MeV and Θ_{lab} = 15°, and

b) ^{38}Ar at E_α = 65 MeV and Θ_{lab} = 13°.

Fig. 7. A spectrum of the ^{36}Ar(α,^{2}He)^{38}Ar reaction at E_α = 65 MeV and Θ_{lab} = 13°.

Fig. 8. A spectrum of the ^{32}S(α,^{2}He)^{34}S reaction at E_α = 65 MeV and Θ_{lab} = 15°.

Fig. 9. Spectra of the (α,^{2}He) reaction at E_α = 65 MeV on:
a) ^{28}Si at Θ_{lab} = 12° (at poorer than normal resolution) and
b) ^{26}Mg at Θ_{lab} = 12.5°.

Fig. 10. A spectrum of the ^{29}Si(α,^{2}He)^{31}Si reaction at E_α = 65 MeV and Θ_{lab} = 12.5°.

Fig. 11. Spectra of the (α,^{2}He) reaction on:

a) ^{24}Mg at E_α = 55 MeV and Θ_{lab} = 12°; and

b) ^{22}Ne at E_α = 65 MeV and Θ_{lab} = 13°.

Fig. 12. Spectra of the $(\alpha, {}^2\text{He})$ reaction at E_α = 65 MeV on:

a) ${}^{20}\text{Ne}$ at Θ_{lab} = 12.5°.

b) ${}^{18}\text{O}$ at Θ_{lab} = 13°.

Fig. 13. Comparison of the calculated and experimental level schemes of ${}^{30}\text{Si}$, ${}^{34}\text{S}$ and ${}^{42}\text{Ca}$. Above the ground states, only the states observed in these experiments are presented.

Fig. 14. Binding energies, B, for one- and two-neutron states possessing several different configurations as a function of the mass of the final nucleus A.

(a) ^{2}He detection system

Beam

θ_{lab}

p_1

p_2

^{2}He → p + p

Collimator

ΔE_1

ΔE_2

E_1

E_2

(b) Δ TOF

Counts

FWHM   1.1 ns

Time (ns)

(c) Calculated
^{2}He detection
efficiency

Efficiency (%)

$E_{2_{He}}$ (MeV)

XBL781-2351

Fig. 1

Fig. 2

XBL 7711-11341

IBL-7157

Fig. 3

Fig. 4

XBL 7711-11345

XBL782-248

Fig. 5

Fig. 6

XBL 7711-11340

Fig. 7

Fig. 8

XBL 7711-11349

IBL-7157

Fig. 9

XBL 7711-11338

Fig. 10

XBL 7711-11335

Fig. 12
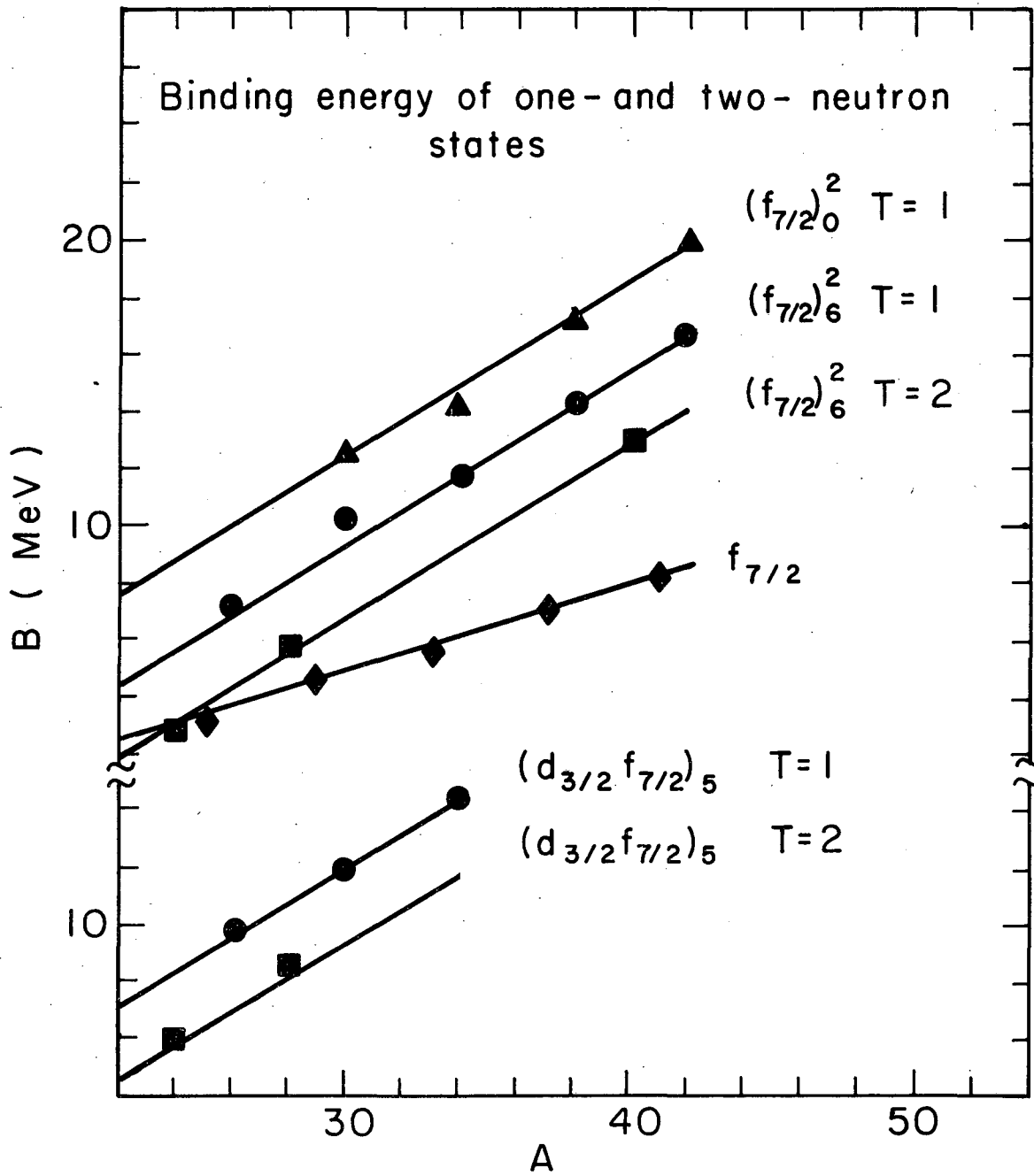
Fig. 13

Fig. 14   XBL 782-247